



Nanoscale

Controlling the Durability and Optical Properties of Triplet-Triplet Annihilation Upconversion Nanocapsules

Journal:	<i>Nanoscale</i>
Manuscript ID	NR-COM-01-2023-000067.R1
Article Type:	Communication
Date Submitted by the Author:	21-Mar-2023
Complete List of Authors:	Schloemer, Tracy; Stanford University, Electrical Engineering Sanders, Samuel; Rowland Institute at Harvard, Narayanan, Pournima; Stanford University, Electrical Engineering; Stanford University, Chemistry Zhou, Qi; Stanford University, Electrical Engineering Hu, Manchen; Stanford University, Electrical Engineering Congreve, Daniel; Stanford University, Electrical Engineering; Rowland Institute at Harvard

SCHOLARONE™
Manuscripts

Controlling the Durability and Optical Properties of Triplet-Triplet Annihilation Upconversion Nanocapsules

Authors: Tracy H. Schloemer^a, Samuel N. Sanders^b, Pournima Narayanan^{a,c}, Qi Zhou^a, Manchen Hu^a, and Daniel N. Congreve^{a,b*}

Affiliations:

^aDepartment of Electrical Engineering, Stanford University, Stanford, CA 94305

^bRowland Institute at Harvard University, Cambridge, MA 02142

^cDepartment of Chemistry, Stanford University, Stanford, CA 94305

*congreve@stanford.edu

Abstract:

Deep penetration of high energy photons by direct irradiation is often not feasible due to absorption and scattering losses, which are generally exacerbated as photon energy increases. Precise generation of high energy photons beneath a surface can circumvent these losses and significantly transform optically controlled processes like photocatalysis or 3D printing. Using triplet-triplet annihilation upconversion (TTA-UC), a nonlinear process, we can locally convert two transmissive low energy photons into one high energy photon. We recently demonstrated the use of nanocapsules for high energy photon generation at depth, with durability within a variety of chemical environments due to the formation of a dense, protective silica shell that prevents content leakage and nanocapsule aggregation. Here, we show the importance of the feed concentrations of the tetraethylorthosilicate monomer (TEOS) and the poly(ethyleneglycol) (PEG) ligand used to synthesize these nanocapsules using spectroscopic and microscopy characterizations. At optimal TEOS and PEG-silane concentrations, minimal nanocapsule leakage can be obtained which maximizes UC photoluminescence. We also spectroscopically study the origin of inefficient upconversion from UCNCs made using sub-optimal conditions to probe how TEOS and PEG-silane concentrations impact the equilibrium between productive shell growth and side product formation, like amorphous silica. Furthermore, this optimized fabrication protocol can be applied to encapsulate multiple TTA-UC systems and other emissive dyes to generate anti-Stokes or Stokes shifted emission, respectively. These results show that simple synthetic controls can be tuned to obtain robust, well-dispersed, bright upconverting nanoparticles for subsequent integration in optically controlled technologies.

Main Text:

All-optical control of photoresponsive materials can transform disparate fields such as photocatalysis, optogenetics, additive manufacturing, and more.^{1–7} Yet in each of these scenarios, it can be challenging to provide the high energy photons typically required for manipulating photochemistry, because these photons do not typically penetrate more than a few microns beyond the surface of a material due to scattering and absorption losses.⁸ Two tactics are generally employed to overcome this barrier: engineering photoresponsive materials to absorb lower, more deeply penetrating wavelengths,^{9–12} or generating the requisite high energy light locally using a nonlinear process.^{13–15} Incredible gains have been made in designing low energy absorbing molecules, yet engineering photoresponsive materials can unpredictably alter other properties.^{1,16} On the other hand, using a nonlinear process can allow for precise high energy photon generation at depth.^{17–21}

One such nonlinear process, triplet-triplet annihilation upconversion (TTA-UC), exploits excitonic states in organic semiconductors to convert two low energy photons into one high energy photon (anti-Stokes shift).^{13,20} Briefly, a sensitizer (typically a metalated porphyrin^{13,17}) absorbs low energy photons, whose energy is transferred to annihilator molecules (often acenes^{13,17}) *via* triplet energy transfer. Two annihilator triplets can fuse by means of triplet-triplet annihilation (TTA) to form an excited singlet exciton.^{22–24} When an excited singlet is formed, it can radiatively decay, emitting a higher energy photon relative to the input light (**Fig. 1A**). TTA-UC has been widely studied, especially in recent years, and there are many sensitizer/annihilator pairs that can efficiently generate upconverted emission under relatively low irradiation power densities, imparting enormous flexibility in input and output wavelength selection.^{17,19,20,25–27}

TTA-UC has been a particularly active research area for a variety of solution-state applications, including photocatalysis,²⁸ biological applications,^{29–31} and additive manufacturing.^{32–34} Integrating TTA-UC materials into a larger-scale application can be challenging, especially because high concentrations of upconversion materials are required to efficiently generate upconverted photons. These high concentrations can introduce other intrinsic energetic challenges and extrinsic challenges.^{17,19,20,25–27} For instance, in solution, the requisite concentrations for efficient TTA-UC leads to significant light attenuation at the surface, even though low energy photons are used. Additionally, commonly used sensitizers and annihilators are typically hydrophobic, limiting solubility to non-polar environments. One extremely successful motif to overcome these challenges has been to encapsulate materials inside of nanoparticles, such as liposomes,^{35–37} polymer-coated nanodroplets,^{38–42} and silica-coated nanoparticles.^{32,43–47} This allows for the TTA-UC materials to be highly concentrated within the nanoparticle, but the nanoparticle concentration can be tuned such that the low energy light can penetrate sufficiently beyond the surface and deliver ample upconverted photons.

When selecting a nanoparticle system, the deployment context must be considered to leverage specific optical and material properties. For instance, polymeric micelles are typically dispersed in aqueous environments,^{38–42} as the micelles will disassemble and release their contents in other non-polar solvents.³² Recently, we engineered silica-coated nanoparticles containing upconversion materials in an oleic acid core for successful dispersion in a variety of polar and non-polar solvents (**Fig. 1B, Fig. S1**).^{32,47} The silica shell protects the structural integrity of the oleic acid core and its

upconverting payload even in solvents where the core is miscible (**Fig. 1C**), and 10,000 g/mol methoxy PEG-silane (PEG-silane) ligands introduce steric bulk, improving nanoparticle solubility and preventing irreversible nanoparticle aggregation and fusion that occurs within an hour.³²

In this study, we examine the reaction dynamics surrounding the formation of the critically important silica shell. Specifically, we show the shell formation is sensitive to the concentration of two key precursors: tetraethyl orthosilicate (TEOS) and PEG-silane. We identify concentration regimes that lead to the formation of capsules with durable shells, and concentration regimes that lead to the formation of thin, leaky shells or to significant aggregation and the relationship of these regimes to the upconverted light output (**Fig. 1D**). We highlight a useful method to assess the nanocapsule durability spectroscopically before full reaction purification, saving time and resources during the rapid prototyping process. Finally, we encapsulate multiple upconversion systems and hydrophobic dyes using the optimized nanocapsule fabrication protocol, demonstrating the protocol's versatility. These findings support the development and deployment of nanocapsules for various applications that require durable encapsulation of hydrophobic payloads.

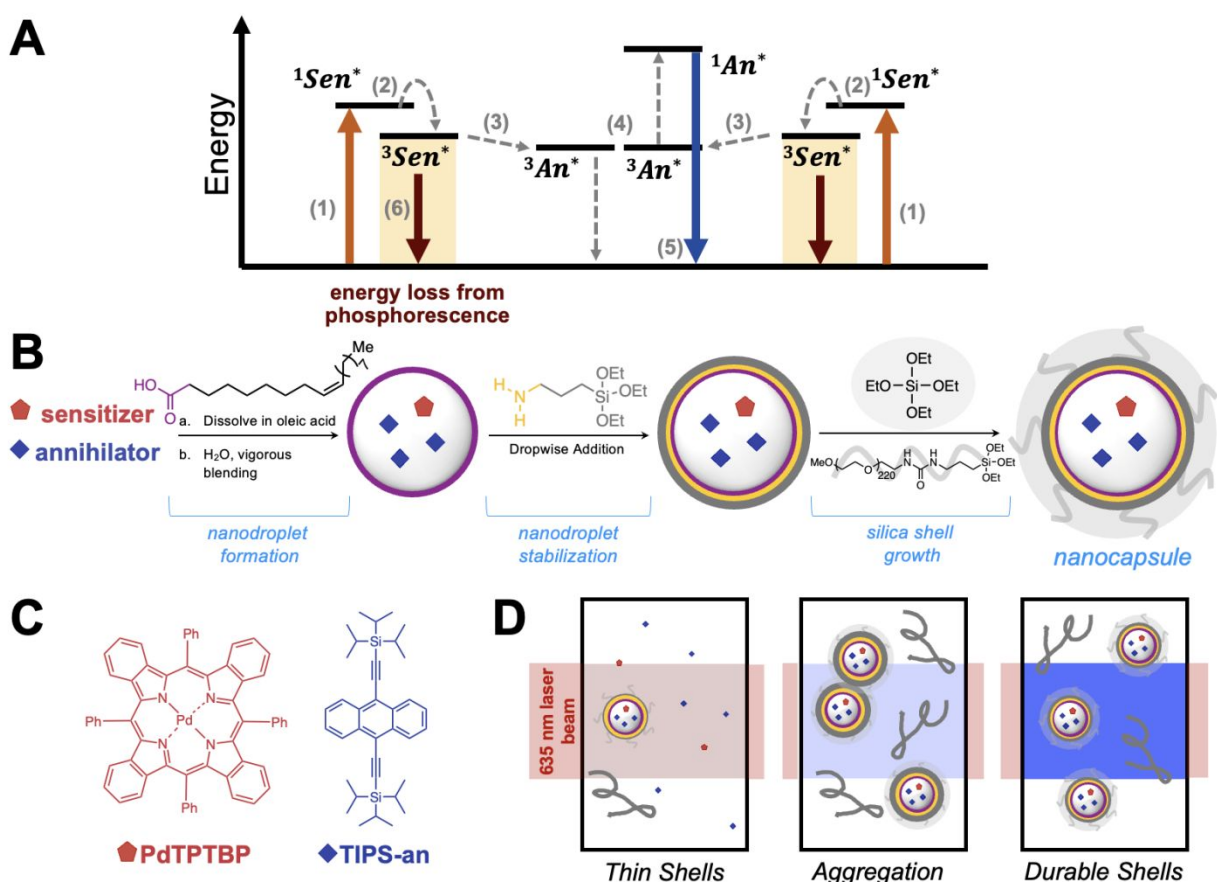


Figure 1: A) A schematic of the triplet-triplet annihilation upconversion mechanism which involves 1) the absorption of two low energy photons (red arrows) by two sensitizer molecules, which are excited to their singlet excited states ($^1\text{Sen}^*$) and 2) intersystem crossing to their triplet excited states ($^3\text{Sen}^*$). These excited sensitizer triplets then 3) transfer their energy to two ground state annihilator molecules by means of a Dexter triplet energy transfer. This excites annihilator

molecules to their triplet states ($^3\text{An}^*$) and the sensitizers return to their ground states. Two annihilators in their triplet states can undergo 4) triplet-triplet annihilation, resulting in one ground state annihilator and one singlet annihilator ($^1\text{An}^*$) which 5) can emit one higher energy photon (anti-Stokes shift, blue arrow) with an energy of less than $2 \times ^3\text{Sen}^*$. 6) Sensitizer triplets can also phosphoresce to the ground state. This loss pathway is emphasized with a yellow box. Sen = sensitizer molecule, An = annihilator molecule, Sen* or An* = excited state, ^1Sen or ^1An = singlet, ^3Sen or ^3An = triplet. B) A summary of the upconversion nanocapsule fabrication. Sensitizer and annihilators are dissolved in oleic acid. Oleic acid nanodroplets are formed *via* vigorous blending and stabilized with (3-aminopropyl)triethoxysilane. Tetraethyl orthosilicate and PEG-silane are added to grow a dense silica shell. This schematic was edited with permission from Ref.³². C) The chemical structures of the sensitizer (PdTPPTBP, palladium (II) *meso*-tetraphenyl tetrabenzoporphine) and annihilator (TIPS-an, 9,10-bis[(triisopropylsilyl)ethynyl]anthracene) used throughout this work. D) A cartoon depiction of upconversion nanocapsules dispersed in acetone and irradiated with a 635 nm laser and the resulting relative intensities of phosphorescence (red) or upconverted emission (blue). From left to right: upconversion nanocapsules with thin shells, with aggregated species (nanocapsules and/or high molecular weight, amorphous silica), and durable shells. The gray wavy lines depict high molecular weight, amorphous silica that is not associated with the nanocapsule silica shell but is generated during the nanocapsule fabrication.

We fabricated upconversion nanocapsules containing palladium (II) *meso*-tetraphenyl tetrabenzoporphine (PdTPPTBP) and 9,10-bis[(triisopropylsilyl)ethynyl]anthracene (TIPS-an), a well-established red-to-blue upconversion system^{32,48} (**Materials and Methods, Table S1, Table S2**). We prepared nanocapsules using a 20 mL scale reaction (**Materials and Methods**), but we emphasize that we have found this preparation to be scalable without adjustment of the relative feedstock ratios (i.e., 20 mL to 200 mL).⁴⁷ The optical densities of the oleic acid stock solutions utilized to make PdTPPTBP/TIPS-an nanocapsules are identical (i.e., the total quantity of sensitizer and annihilator added to make nanocapsules are equivalent). To study the ensemble nanocapsule quality as a function of feedstock, we strategically analyzed small aliquots from the crude reactions and quantified the upconverted emission relative to the phosphorescence of the sensitizer, PdTPPTBP. Monitoring the upconversion and phosphorescence emission (under 635 nm excitation) provides constructive insights due to the quadratic nature of TTA-UC: upconverted emission is observed when the sensitizer and annihilator are contained within the nanocapsules, as the concentrations within each nanocapsule is high enough for efficient energy transfer, leading to bright blue upconverted emission. By diluting the reaction aliquot by 100x v/v in acetone, we can be confident that the sensitizer and annihilator concentrations are extremely low. Therefore, if the silica shell has not sufficiently encapsulated the oleic acid nanodroplet, the oleic acid and its contents will dissolve in acetone and sensitizer phosphorescence will be observed due to inefficient triplet energy transfer from the sensitizer to the annihilator (**Fig. 1D**). In contrast, direct excitation to monitor the annihilator fluorescence (Stokes shift) can provide less information regarding the presence of the encapsulated versus free-floating materials without further reaction purification due to the annihilator's high photoluminescent quantum yield.⁴⁸ Of course, not all oleic acid nanodroplets in a given batch possess silica shells with the same durability, as the shell growth relies on numerous substitution reactions in a step-growth fashion (**Figure S1**),^{49–51} but overall, the ratio of UC emission and phosphorescence provides a rapid and simple method to assess the majority quality of the nanocapsules. Since we have previously observed bright upconverted

emission from nanocapsules dispersed in a variety of organic solvents,³² we select acetone as a cost-effective, simple proxy to predict durability in other organic solvents or other complex environments, such as a 3D printing resin.

First, we investigated the effects of TEOS loading on nanocapsule formation, and find the TEOS concentration has significant impacts on nanocapsule durability and UC light output. Upon irradiation with 635 nm at extremely low TEOS loadings (0-0.8 mL), only sensitizer phosphorescence is observed both by eye (**Fig. 2A-B**) as well as spectroscopically (**Fig. 3A, Table S3**), signifying a considerable population of these nanocapsules release their contents in acetone. Still, the presence of some durable nanocapsules at low TEOS loadings is confirmed by dynamic light scattering (DLS). When as little as 0.4 mL TEOS is used during fabrication, a small fraction of intact nanocapsules is present when the DLS sample is diluted in acetone, even though UC emission is not observed (**Table S4, Fig. S2**). Since no UC emission is observed, it can be inferred that the nanocapsule concentration is much lower compared to samples where bright upconverted emission is observed under the same conditions.

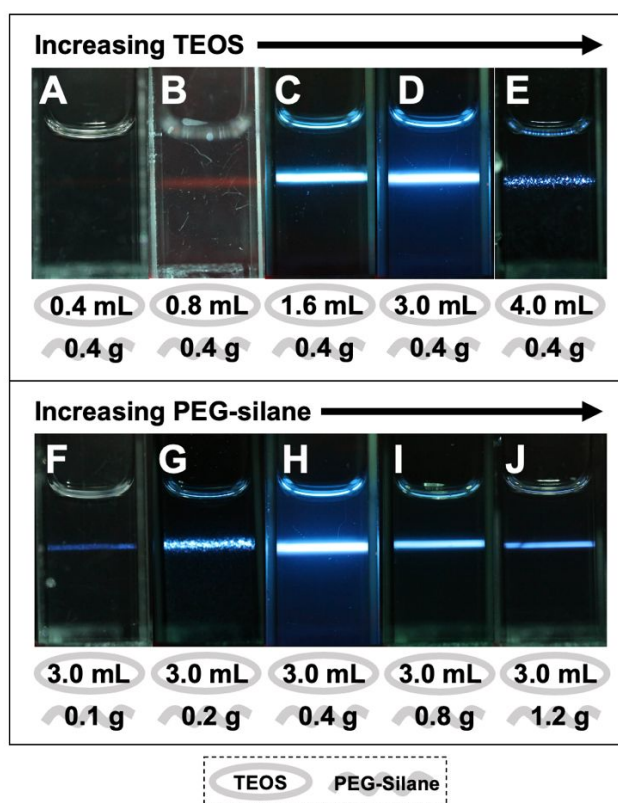


Figure 2: A-I) Photographs of upconversion nanocapsules synthesized with varying quantities of tetraethyl orthosilicate and PEG-silane on a 20 mL scale. Crude reaction aliquots were diluted 100x in acetone, irradiated with a 635 nm laser over a pathlength of 10 mm at 66 W cm⁻², and imaged through a 600 nm shortpass filter. Panel D is repeated in panel H for continuity within the increasing PEG-silane series.

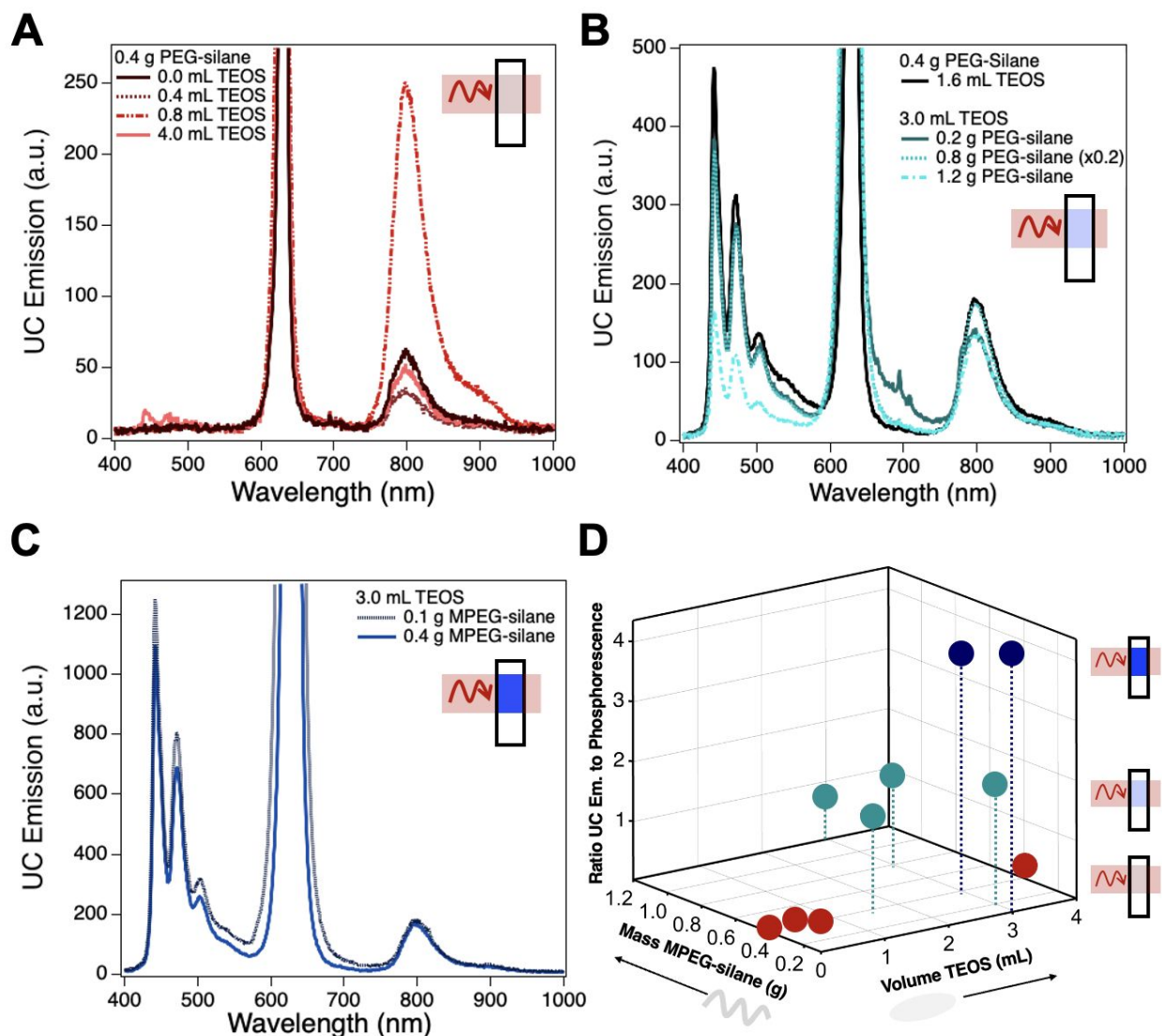


Figure 3: A-C) The upconversion photoluminescence spectra of the upconversion nanocapsule samples depicted in Fig. 2, grouped by the ratio of UC emission at 474 nm: sensitizer phosphorescence at 800 nm (A = UC emission:phosphorescence < 0.5, B = 0.5 < UC emission:phosphorescence < 3, and C = UC emission:phosphorescence > 3). TIPS-an upconversion emission is observed from 450-550 nm and PdTPTBP phosphorescence is observed from 750-850 nm. The peak centered at 635 nm originates from laser scatter. Note that the y-axes are scaled differently in each panel. D) Correlating TEOS and PEG-silane loadings to the ratio of UC emission to sensitizer phosphorescence presented in panels A-C and Table S3.

At moderate TEOS loadings (1.6-3.0 mL), bright upconversion emission is easily observed by eye (Fig. 2C-D). With 3.0 mL TEOS, the observed UC photons are approximately double those observed when 1.6 mL TEOS is added (Fig. 3B-C, Table S3). We estimate the TEOS volume consumed to make nanocapsule shells is roughly on the order of 1 mL at this scale (Table S5). Since some TEOS is consumed in nanocapsule growth and some is consumed to produce high molecular weight silica, it is reasonable that at TEOS loadings of approximately 1 mL, a decent

population of stable nanocapsules can successfully form which results in bright upconverted emission. Beyond 3.0 mL of TEOS, upconverted emission is still observed, but there is also significantly increased optical scatter likely due to aggregated nanocapsules and large molecular weight silica (**Fig. 2E, Fig. 3A, Table S3**). Thus, the TEOS loading plays a crucial role in outcome of two competing processes: silica growth from the nanocapsule surface and silica growth to produce large molecular weight species. This aligns well with the well-established knowledge that the kinetics of silica growth in solution are extremely sensitive to the ratio of water/TEOS, pH, and temperature.^{49–51}

Varying the PEG-silane loading provides further insight on the nanocapsule shell formation. At low PEG-silane loadings (<0.4 g), only modest upconversion signals are observed (**Fig. 2F-G, Fig. 3B-C**) and significant scatter is evident by eye. This was an expected result, because we have previously shown the PEG-silane's steric bulk is crucial to prevent high molecular weight species from forming within 10s of minutes and irreversibly precipitating.³² However, at loadings beyond 0.4 g, the upconverted emission was unexpectedly dim (**Fig. 2I-J, Fig. 3B**), even though the concentration of silane does not substantially change with an increase in polymer loading. The cartoon depiction of nanocapsule shell growth in **Fig. S1** ignores the contributions of oligomeric species and cyclic species that contribute to silica growth, but these species likely play a significant role in the silica shell formation. We hypothesize that at PEG-silane loadings beyond 0.4 g, the population of oligomeric species that can graft onto a nanocapsule shell is reduced due to the polymer's steric bulk, ultimately reducing the population of durable nanocapsules as observed in **Fig. 2I-J**.

Throughout this nanocapsule fabrication, we found quantifying the ratio of UC emission to PdTPBP phosphorescence to be a useful metric to select the champion fabrication conditions that maximizes UC emission and minimizes sensitizer phosphorescence (**Fig. 3D, Table S3**). By examining the ratio of these two quantities, light scattering impacts are also considered, most useful for categorizing the most highly scattering samples (i.e., **Fig. 2I**). The ratio of UC emission to phosphorescence changes dramatically as a function of TEOS and PEG-silane feeds. For instance, as the TEOS loading increases from 1.6 mL to 3.0 mL at a constant PEG-silane feed mass, the ratio of upconverted emission to phosphorescence emission nearly doubles, increasing from ~2:1 to 4:1. In contrast, the ratio of upconverted emission to sensitizer phosphorescence in the oleic acid solution used to prepare the nanocapsules is ~3:1 (**Fig. S3**). This emphasizes the heterogeneous nature of the contents of the upconversion nanocapsules, where solutes are not equally dispersed among all nanodroplets,^{52,53} and the corresponding differences in observed optical properties resulting from changes in local sensitizer and annihilator concentrations.

These trends are also confirmed after the isolation of upconversion nanocapsules by centrifugation (**Fig. S4**), where high molecular weight species are removed. This is achieved with two centrifugations. First, high molecular weight species are removed by discarding the precipitated solid after a 1-hour spin. Then, the supernatant is further centrifuged over 12-14 hours to isolate a paste comprised of water and nanocapsules, which is further diluted in water and acetone. In contrast to the spectra presented **Fig. 3**, upconverted emission was observed in all samples after >12 hours of centrifugation. Samples prepared with either 1.6 or 3.0 mL TEOS with 0.4 g PEG-silane provided the highest density of durable, isolable upconversion nanocapsules. All other

isolated samples confirm the findings presented in **Figs. 2-3**: a significantly smaller population of durable nanocapsules were produced outside of these optimal conditions.

DLS of the reaction crude diluted in water allowed for us to probe the average hydrodynamic diameters of the nanocapsules formed over the course of the reaction (species >220 nm were removed before measurement using a syringe filter). The average hydrodynamic diameters of the nanocapsules were ~80-95 nm on average except for samples containing <0.4 g PEG-silane (**Table S6, Fig. S5**). For both samples with <0.4 g PEG-silane, the average diameters were 110-150 nm, signifying nanocapsule fusion is occurring without the steric bulk provided by the PEG ligand. We note that free-floating PEG-silane is not detectible in solution, as the hydrodynamic diameter of the free-floating polymer is <5 nm (**Table S7**).

Nanocapsule morphology was also characterized by atomic force microscopy (AFM). While we have previously used scanning electron microscopy for imaging, working under ambient pressures is advantageous to collect multiple measurements without observing nanocapsule fusion.⁴⁷ Representative AFM scans and size distribution statistics are presented in **Figs. 4-5**. Surprisingly, the nanocapsules appear anisotropic by AFM (i.e., larger in diameter than in height), but this may be an artifact of the nanocapsules fusing to the glass substrate's silica surface. For simplicity, we will discuss the apparent diameters, knowing they are possibly a slight overestimate. Hydrodynamic diameters estimated by DLS are also shown in **Fig. 5**.

By AFM, the nanocapsules are relatively small in samples with <1.6 mL TEOS and 0.4 g PEG-silane (~60 nm; **Fig. 4A-B** and **Fig. 5A-B**) compared to samples containing more durable capsules (~85-100 nm; **Fig. 4C-D** and **Fig. 5C-D**). All DLS measurements fall within one standard deviation of the AFM measurements signifying decent agreement among measurement techniques. The average nanocapsule diameters are similar in other samples (**Fig. 4E-F** and **Fig. 5E-F**). In all samples, evidence of amorphous silica is observed (emphasized in **Fig. 4E**). While one cannot make direct comparisons on the concentration of amorphous silica from sample to sample by AFM, we note samples for **Fig. 4A-B** had to be further diluted before measurements (**Materials and Methods**) due to particle aggregation which may be facilitated by the amorphous silica. All in all, AFM provides important insights on the morphology as function of TEOS and PEG-silane loading.

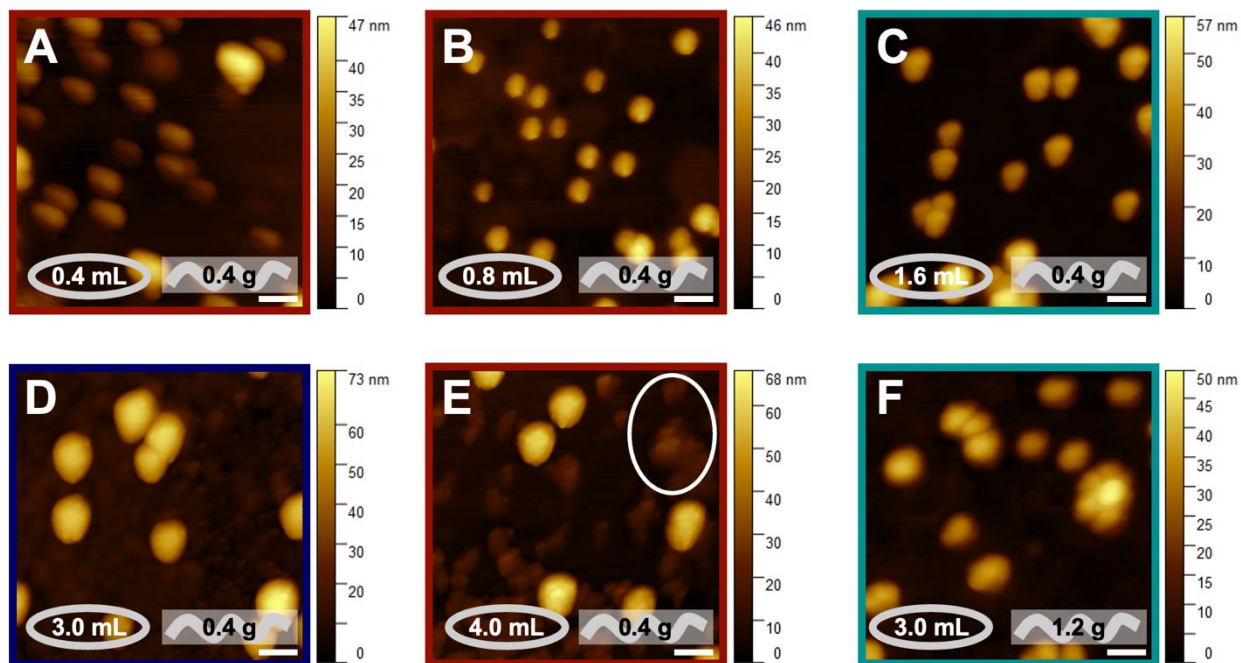


Figure 4: A-F) Representative Atomic Force Microscopy (AFM) of upconversion nanocapsules synthesized with varying quantities of tetraethyl orthosilicate and PEG-silane. The scale bar represents 100 nm. The colored boxes around each panel correspond to the color scheme presented in **Fig. 3** (A,B,E = red = UC emission:phosphorescence < 0.5, C,F = teal = 0.5 < UC emission:phosphorescence < 3, and D = blue = UC emission:phosphorescence > 3). In panel E, the white circle emphasizes the presence of amorphous silica.

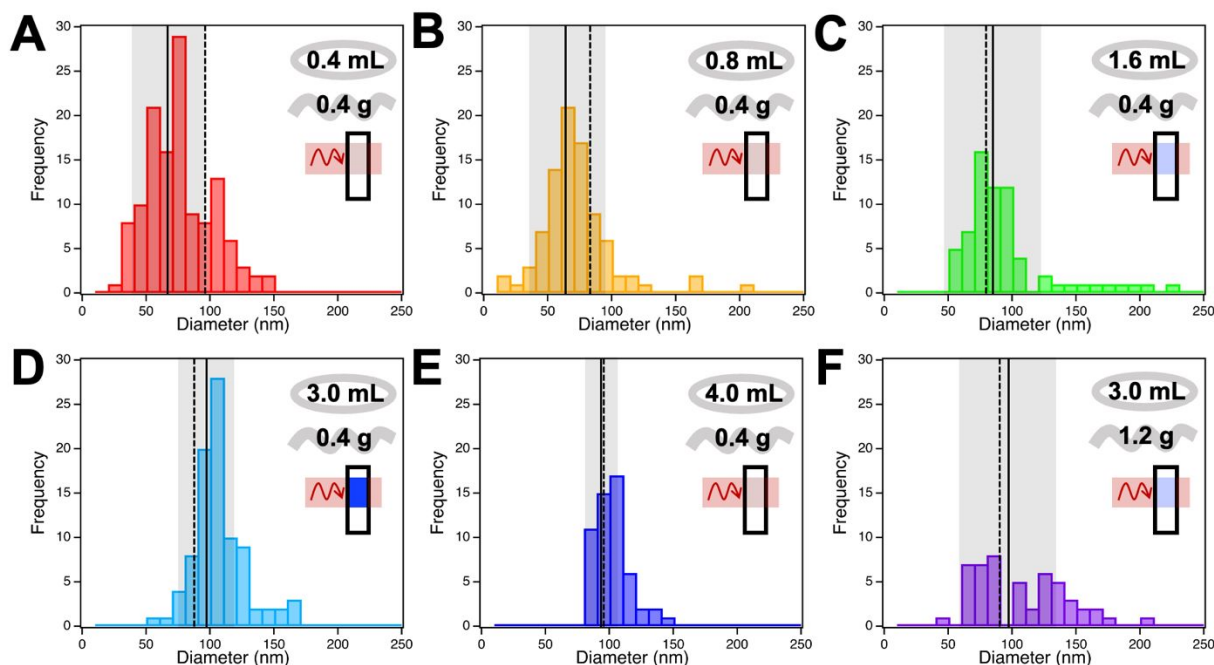


Figure 5: Histograms of the extracted nanocapsule diameters from AFM measurements. The solid vertical line and gray box represents the average nanocapsule diameter and the standard deviation respectively (A= 66 ± 26 nm, B= 62 ± 29 nm, C= 84 ± 37 nm, D = 97 ± 20 nm, E = 91 ± 13 , F= 97 ± 36 nm). The dashed vertical line represents the average nanocapsule hydrodynamic diameter as determined by DLS (**Table S6**). The standard deviations for the DLS measurements are not shown graphically because they are similar in magnitude to the thickness of the dashed vertical line.

Finally, this optimized synthetic process using 3.0 mL TEOS and 0.4 g PEG-silane is not limited to encapsulating only TIPS-an and PdTPTBP. We successfully encapsulated tetra-*tert*-butylperylene (TTBP) and 9,10-bis(phenylethynyl)anthracene (BPEA) with PdTPTBP, as well as BrDPA (2-bromo-9,10-diphenylanthracene) with PtOEP (platinum (II) octaethylporphyrin) for green-to-violet upconversion nanocapsules (**Fig. 6**). We selected BrDPA because its solubility in oleic acid is much larger than the prototypical annihilator paired with PtOEP, 9,10-diphenylanthracene, thus ensuring a larger population of nanocapsules contained adequate annihilator.⁵⁴ Nanocapsules containing PdTPTBP/TTBP or PdTPTBP/TIPS-an displayed similar size distributions by DLS (**Table S8, Fig. S6**). Nanocapsules containing PtOEP/BrDPA or PdTPTBP/BPEA were slightly larger on average with a larger polydispersity index compared to nanocapsules prepared in the same fashion with PdTPTBP/TIPS-an or PdTPTBP/TTBP. While still smaller than reported size distributions for other similar nanoparticles,^{44,45} it suggests that the emulsification process can be moderately sensitive to the molecular identity of solutes in oleic acid.

In addition to encapsulating materials for anti-Stokes emission, we also encapsulated commonly used hydrophobic dyes for imaging using the Stokes emission (**Fig. S7**). Coumarin 30, Coumarin 153, BODIPY 505/515, and a diketopyrrolopyrrole (2,5-Bis(2-ethylhexyl)-3,6-di(furan-2-yl)pyrrolo[3,4-c]pyrrole-1,4(2H,5H)-dione, DPP) were successfully encapsulated. The emission

of Coumarin 30 and BODIPY 505/515 were similar in solution to what was observed from material inside of the nanocapsules. Interestingly, a red shift in the emission is observed in nanocapsules containing Coumarin 153, and DPP emission features broaden compared to the emission observed from unencapsulated materials dissolved in THF or oleic acid, suggesting material aggregation within nanocapsules. Again, there is variation in the observed nanocapsule average hydrodynamic diameter (**Table S9**, **Figure S8**). Encapsulating hydrophobic dyes in nanocapsules allows for their use in many types of environments without the need to synthesize new dyes with tailored solubilities.

Predicting whether a molecule can be encapsulated in these nanoparticles is still underexplored. The materials we successfully encapsulated encompass a wide parameter space with regard to molecular motifs (i.e., acenes, metalated porphyrins, coumarins, BODIPY, DPP). Generally, we find sensitizers and annihilators must be sufficiently soluble in oleic acid and insoluble in water for effective nanoencapsulation. We quantified the partition coefficients of each material dissolved in oleic acid. None of these materials partition into the water layer by UV-Vis spectroscopy (**Fig. S9**). Still, this finding does not necessarily preclude the encapsulation of materials that are soluble in both water and oleic acid.

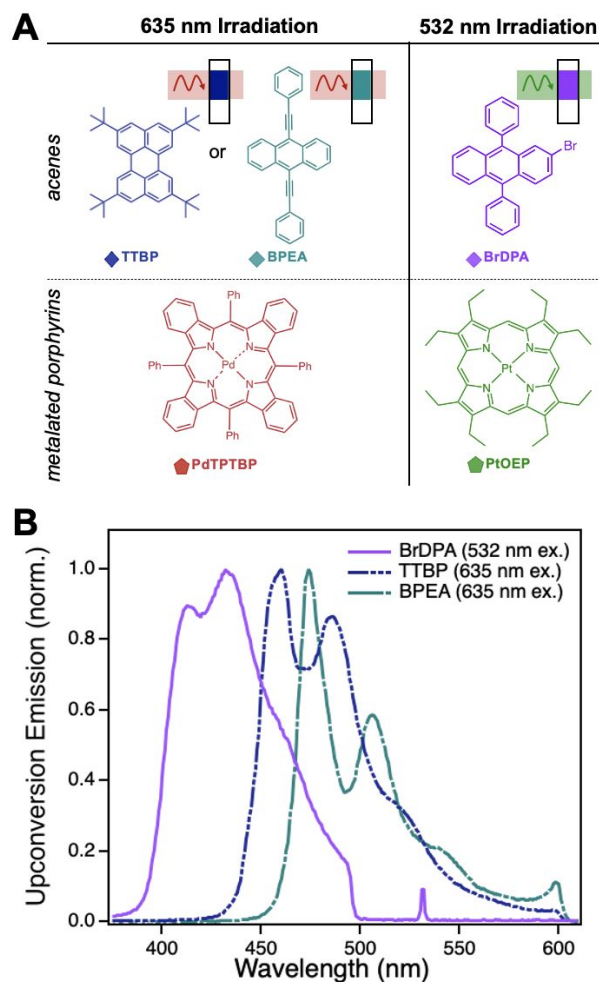


Figure 6: A) Chemical structures of sensitizers and annihilators encapsulated in nanocapsules. B) Normalized upconversion emission of nanocapsules containing PtOEP/DPA (purple), PdTPTBP/TTBP (blue), or PdTPTBP/BPEA (green). Nanocapsules were diluted in water and acetone, and spectra were collected through either a 500 nm (sample with PtOEP) or a 600 nm shortpass filter (samples with PdTPTBP).

In conclusion, the fabrication of durable, bright upconversion nanocapsules is highly dependent upon the TEOS and PEG-silane loadings during preparation. Outside of optimal loadings of 3.0 mL TEOS and 0.4 g PEG-silane on a 20 mL reaction scale, both the absolute upconverted emission and the ratio of upconverted emission to phosphorescence decreases. The losses in the upconverted emission originate from a combination of factors. At low TEOS feed volumes, silica shells are relatively thin, resulting in leaky nanocapsules upon dispersion in acetone, a proxy for core-solvating environments. At high TEOS or PEG-silane feed quantities, the formation of high molecular weight silica significantly increases, which decreases the quantity of durable nanocapsules. This fabrication protocol can be easily tailored to encapsulate different materials to obtain anti-Stokes emission or Stokes emission, as long as the encapsulated molecules are sufficiently soluble in oleic acid and insoluble in water. With a library of durable, optically

responsive nanocapsules, we anticipate they can be used for a myriad of light-controlled applications.

Competing Interests: S.N.S. and D.N.C are co-founders of Quadratic3D, Inc. S.N.S. is the Chief Technological Officer and D.N.C. is the Chief Scientific Advisor.

Funding: This research is funded through the support of the Rowland Fellowship at the Rowland Institute at Harvard University, the Harvard PSE Accelerator Fund, and the Gordon and Betty Moore Foundation, and the Department of Electrical Engineering at Stanford University. A portion of this work was performed at the Harvard Center for Nanoscale Systems (CNS), a member of the National Nanotechnology Coordinated Infrastructure Network (NNCI), which is supported by the National Science Foundation under NSF, Award No. 1541959. A portion of this work was performed at the Stanford Nano Shared Facilities (SNSF), supported by the National Science Foundation under award ECCS-2026822. A portion of this work was performed at the Stanford ChEM-H Macromolecular Structure Knowledge Center.

Acknowledgements: T.H.S. and S.N.S. acknowledge the support of Arnold O. Beckman Postdoctoral Fellowships. P. N. acknowledges the support of a Stanford Graduate Fellowship in Science & Engineering (SGF) as a Gabilan Fellow. We thank Daniel Anderson for the fruitful discussions regarding nanocapsule characterization and the Mai lab for the use of their Sorvall X4 Pro Centrifuge.

References:

- (1) Goulet-Hanssens, A.; Eisenreich, F.; Hecht, S. Enlightening Materials with Photoswitches. *Adv. Mater.* **2020**, *32* (20), 1905966. <https://doi.org/10.1002/adma.201905966>.
- (2) *Molecular Photoswitches. Volume 1*; Pianowski, Z. L., Ed.; Wiley-VCH: Weinheim, 2022.
- (3) Yang, X.; Wang, D. Photocatalysis: From Fundamental Principles to Materials and Applications. *ACS Appl. Energy Mater.* **2018**, *1* (12), 6657–6693. <https://doi.org/10.1021/acsaem.8b01345>.
- (4) Shen, Y.; Campbell, R. E.; Côté, D. C.; Paquet, M.-E. Challenges for Therapeutic Applications of Opsin-Based Optogenetic Tools in Humans. *Front. Neural Circuits* **2020**, *14*.
- (5) Ligon, S. C.; Liska, R.; Stampfl, J.; Gurr, M.; Mülhaupt, R. Polymers for 3D Printing and Customized Additive Manufacturing. *Chem. Rev.* **2017**, *117* (15), 10212–10290. <https://doi.org/10.1021/acs.chemrev.7b00074>.
- (6) Bagheri, A.; Jin, J. Photopolymerization in 3D Printing. *ACS Appl. Polym. Mater.* **2019**, *1* (4), 593–611. <https://doi.org/10.1021/acsapm.8b00165>.
- (7) Regehly, M.; Garmshausen, Y.; Reuter, M.; König, N. F.; Israel, E.; Kelly, D. P.; Chou, C.-Y.; Koch, K.; Asfari, B.; Hecht, S. Xolography for Linear Volumetric 3D Printing. *Nature* **2020**, *588* (7839), 620–624. <https://doi.org/10.1038/s41586-020-3029-7>.
- (8) Henderson, T. A.; Morries, L. D. Near-Infrared Photonic Energy Penetration: Can Infrared Phototherapy Effectively Reach the Human Brain? *Neuropsychiatr. Dis. Treat.* **2015**, *11*, 2191–2208. <https://doi.org/10.2147/NDT.S78182>.

- (9) Corrigan, N.; Ciftci, M.; Jung, K.; Boyer, C. Mediating Reaction Orthogonality in Polymer and Materials Science. *Angew. Chem. Int. Ed.* **2021**, *60* (4), 1748–1781. <https://doi.org/10.1002/anie.201912001>.
- (10) Truong, V. X.; Ehrmann, K.; Seifermann, M.; Levkin, P. A.; Barner-Kowollik, C. Wavelength Orthogonal Photodynamic Networks. *Chem. – Eur. J.* **2022**, *28* (25), e202104466. <https://doi.org/10.1002/chem.202104466>.
- (11) Friedman, H. C.; Cosco, E. D.; Atallah, T. L.; Jia, S.; Sletten, E. M.; Caram, J. R. Establishing Design Principles for Emissive Organic SWIR Chromophores from Energy Gap Laws. *Chem* **2021**, *0* (0). <https://doi.org/10.1016/j.chempr.2021.09.001>.
- (12) Jia, S.; Lin, E.; Lim, I.; Mobley, E.; Guo, L.; Sletten, E. *Water Soluble Chromenylum Dyes for Shortwave Infrared Imaging in Mice*; preprint; Chemistry, 2022. <https://doi.org/10.26434/chemrxiv-2022-h8rjb>.
- (13) Singh-Rachford, T. N.; Castellano, F. N. Photon Upconversion Based on Sensitized Triplet–Triplet Annihilation. *Coord. Chem. Rev.* **2010**, *254* (21), 2560–2573. <https://doi.org/10.1016/j.ccr.2010.01.003>.
- (14) Yang, W.; Li, X.; Chi, D.; Zhang, H.; Liu, X. Lanthanide-Doped Upconversion Materials: Emerging Applications for Photovoltaics and Photocatalysis. *Nanotechnology* **2014**, *25* (48), 482001. <https://doi.org/10.1088/0957-4484/25/48/482001>.
- (15) Weingarten, D. H.; LaCount, M. D.; van de Lagemaat, J.; Rumbles, G.; Lusk, M. T.; Shaheen, S. E. Experimental Demonstration of Photon Upconversion via Cooperative Energy Pooling. *Nat. Commun.* **2017**, *8* (1), 14808. <https://doi.org/10.1038/ncomms14808>.
- (16) Boelke, J.; Hecht, S. Designing Molecular Photoswitches for Soft Materials Applications. *Adv. Opt. Mater.* **2019**, *7* (16), 1900404. <https://doi.org/10.1002/adom.201900404>.
- (17) Zhou, J.; Liu, Q.; Feng, W.; Sun, Y.; Li, F. Upconversion Luminescent Materials: Advances and Applications. *Chem. Rev.* **2015**, *115* (1), 395–465. <https://doi.org/10.1021/cr400478f>.
- (18) Chen, G.; Qiu, H.; Prasad, P. N.; Chen, X. Upconversion Nanoparticles: Design, Nanochemistry, and Applications in Theranostics. *Chem. Rev.* **2014**, *114* (10), 5161–5214. <https://doi.org/10.1021/cr400425h>.
- (19) Ahmad, W.; Wang, J.; Li, H.; Ouyang, Q.; Wu, W.; Chen, Q. Strategies for Combining Triplet–Triplet Annihilation Upconversion Sensitizers and Acceptors in a Host Matrix. *Coord. Chem. Rev.* **2021**, *439*, 213944. <https://doi.org/10.1016/j.ccr.2021.213944>.
- (20) Zeng, L.; Huang, L.; Han, J.; Han, G. Enhancing Triplet–Triplet Annihilation Upconversion: From Molecular Design to Present Applications. *Acc. Chem. Res.* **2022**, *55* (18), 2604–2615. <https://doi.org/10.1021/acs.accounts.2c00307>.
- (21) Schloemer, T.; Narayanan, P.; Zhou, Q.; Belliveau, E.; Seitz, M.; Congreve, D. N. Nanoengineering Triplet–Triplet Annihilation Upconversion: From Materials to Real-World Applications. *ACS Nano* **2023**, acsnano.3c00543. <https://doi.org/10.1021/acsnano.3c00543>.
- (22) Saltiel, J.; Atwater, B. W. Spin-Statistical Factors in Diffusion-Controlled Reactions. In *Advances in Photochemistry*; Volman, D. H., Hammond, G. S., Gollnick, K., Eds.; John Wiley & Sons, Inc.: Hoboken, NJ, USA, 2007; pp 1–90. <https://doi.org/10.1002/9780470133446.ch1>.
- (23) Bharmoria, P.; Bildirir, H.; Moth-Poulsen, K. Triplet–Triplet Annihilation Based near Infrared to Visible Molecular Photon Upconversion. *Chem. Soc. Rev.* **2020**, *49* (18), 6529–6554. <https://doi.org/10.1039/D0CS00257G>.

- (24) Bossanyi, D. G.; Sasaki, Y.; Wang, S.; Chekulaev, D.; Kimizuka, N.; Yanai, N.; Clark, J. Spin Statistics for Triplet–Triplet Annihilation Upconversion: Exchange Coupling, Intermolecular Orientation, and Reverse Intersystem Crossing. *JACS Au* **2021**, *1* (12), 2188–2201. <https://doi.org/10.1021/jacsau.1c00322>.
- (25) Rauch, M. P.; Knowles, R. R. Applications and Prospects for Triplet–Triplet Annihilation Photon Upconversion. *Chim. Int. J. Chem.* **2018**, *72* (7), 501–507. <https://doi.org/10.2533/chimia.2018.501>.
- (26) Gray, V.; Moth-Poulsen, K.; Albinsson, B.; Abrahamsson, M. Towards Efficient Solid-State Triplet–Triplet Annihilation Based Photon Upconversion: Supramolecular, Macromolecular and Self-Assembled Systems. *Coord. Chem. Rev.* **2018**, *362*, 54–71. <https://doi.org/10.1016/j.ccr.2018.02.011>.
- (27) Seo, S. E.; Choe, H.-S.; Cho, H.; Kim, H.; Kim, J.-H.; Kwon, O. S. Recent Advances in Materials for and Applications of Triplet–Triplet Annihilation-Based Upconversion. *J. Mater. Chem. C* **2022**, 10.1039.D1TC03551G. <https://doi.org/10.1039/D1TC03551G>.
- (28) Ravetz, B. D.; Pun, A. B.; Churchill, E. M.; Congreve, D. N.; Ravis, T.; Campos, L. M. Photoredox Catalysis Using Infrared Light via Triplet Fusion Upconversion. *Nature* **2019**, *565* (7739), 343–346. <https://doi.org/10.1038/s41586-018-0835-2>.
- (29) Askes, S. H. C.; Kloz, M.; Bruylants, G.; Kennis, J. T. M.; Bonnet, S. Triplet–Triplet Annihilation Upconversion Followed by FRET for the Red Light Activation of a Photodissociative Ruthenium Complex in Liposomes. *Phys. Chem. Chem. Phys.* **2015**, *17* (41), 27380–27390. <https://doi.org/10.1039/C5CP04352B>.
- (30) Askes, S. H. C.; Pomp, W.; Hopkins, S. L.; Kros, A.; Wu, S.; Schmidt, T.; Bonnet, S. Imaging Upconverting Polymersomes in Cancer Cells: Biocompatible Antioxidants Brighten Triplet–Triplet Annihilation Upconversion. *Small* **2016**, *12* (40), 5579–5590. <https://doi.org/10.1002/sml.201601708>.
- (31) Liu, Q.; Wang, W.; Zhan, C.; Yang, T.; Kohane, D. S. Enhanced Precision of Nanoparticle Phototargeting in Vivo at a Safe Irradiance. *Nano Lett.* **2016**, *16* (7), 4516–4520. <https://doi.org/10.1021/acs.nanolett.6b01730>.
- (32) Sanders, S. N.; Schloemer, T. H.; Gangishetty, M. K.; Anderson, D.; Seitz, M.; Gallegos, A. O.; Stokes, R. C.; Congreve, D. N. Triplet Fusion Upconversion Nanocapsules for Volumetric 3D Printing. *Nature* **2022**, *604* (7906), 474–478. <https://doi.org/10.1038/s41586-022-04485-8>.
- (33) Limberg, D. K.; Kang, J.-H.; Hayward, R. C. Triplet–Triplet Annihilation Photopolymerization for High-Resolution 3D Printing. *J. Am. Chem. Soc.* **2022**, jacs.1c11022. <https://doi.org/10.1021/jacs.1c11022>.
- (34) Wang, Z.; Hou, Y.; Huo, Z.; Liu, Q.; Xu, W.; Zhao, J. Spatially Confined Photoexcitation with Triplet–Triplet Annihilation Upconversion. *Chem. Commun.* **2021**, 10.1039.D1CC03309C. <https://doi.org/10.1039/D1CC03309C>.
- (35) Askes, S. H. C.; Bahreman, A.; Bonnet, S. Activation of a Photodissociative Ruthenium Complex by Triplet–Triplet Annihilation Upconversion in Liposomes. *Angew. Chem. Int. Ed.* **2014**, *53* (4), 1029–1033. <https://doi.org/10.1002/anie.201309389>.
- (36) Kouno, H.; Ogawa, T.; Amemori, S.; Mahato, P.; Yanai, N.; Kimizuka, N. Triplet Energy Migration-Based Photon Upconversion by Amphiphilic Molecular Assemblies in Aerated Water. *Chem. Sci.* **2016**, *7* (8), 5224–5229. <https://doi.org/10.1039/C6SC01047D>.

- (37) Mattiello, S.; Monguzzi, A.; Pedrini, J.; Sassi, M.; Villa, C.; Torrente, Y.; Marotta, R.; Meinardi, F.; Beverina, L. Self-Assembled Dual Dye-Doped Nanosized Micelles for High-Contrast Up-Conversion Bioimaging. *Adv. Funct. Mater.* **2016**, *26* (46), 8447–8454. <https://doi.org/10.1002/adfm.201603303>.
- (38) Wohnhaas, C.; Turshatov, A.; Mailänder, V.; Lorenz, S.; Balushev, S.; Miteva, T.; Landfester, K. Annihilation Upconversion in Cells by Embedding the Dye System in Polymeric Nanocapsules: Annihilation Upconversion in Cells by Embedding *Macromol. Biosci.* **2011**, *11* (6), 772–778. <https://doi.org/10.1002/mabi.201000451>.
- (39) Kim, J.-H.; Kim, J.-H. Triple-Emulsion Microcapsules for Highly Efficient Multispectral Upconversion in the Aqueous Phase. *ACS Photonics* **2015**, *2* (5), 633–638. <https://doi.org/10.1021/acsp Photonics.5b00042>.
- (40) Kang, J.-H.; Lee, S. S.; Guerrero, J.; Fernandez-Nieves, A.; Kim, S.-H.; Reichmanis, E. Ultrathin Double-Shell Capsules for High Performance Photon Upconversion. *Adv. Mater.* **2017**, *29* (21), 1606830. <https://doi.org/10.1002/adma.201606830>.
- (41) Sanders, S. N.; Gangishetty, M. K.; Sfeir, M. Y.; Congreve, D. N. Photon Upconversion in Aqueous Nanodroplets. *J. Am. Chem. Soc.* **2019**, *141* (23), 9180–9184. <https://doi.org/10.1021/jacs.9b03992>.
- (42) Yang, H.; Guo, S.; Jin, B.; Luo, Y.; Li, X. Versatile, Stable, and Air-Tolerant Triplet–Triplet Annihilation Upconversion Block Copolymer Micelles. *Polym. Chem.* **2022**. <https://doi.org/10.1039/D2PY00596D>.
- (43) Liu, Q.; Yang, T.; Feng, W.; Li, F. Blue-Emissive Upconversion Nanoparticles for Low-Power-Excited Bioimaging in Vivo. *J. Am. Chem. Soc.* **2012**, *134* (11), 5390–5397. <https://doi.org/10.1021/ja3003638>.
- (44) Kwon, O. S.; Kim, J.-H.; Cho, J. K.; Kim, J.-H. Triplet–Triplet Annihilation Upconversion in CdS-Decorated SiO₂ Nanocapsules for Sub-Bandgap Photocatalysis. *ACS Appl. Mater. Interfaces* **2015**, *7* (1), 318–325. <https://doi.org/10.1021/am506233h>.
- (45) Quaglia, G.; Bartolomei, B.; Gentili, P. L.; Latterini, L. UV-Visible Radiation Modulation Abilities of Photon up-Converting Nanocapsules Integrated with an Oscillatory Reaction. *J. Mater. Chem. C* **2022**, *10* (23), 9073–9080. <https://doi.org/10.1039/D2TC00709F>.
- (46) Askes, S. H. C.; Leeuwenburgh, V. C.; Pomp, W.; Arjmandi-Tash, H.; Tanase, S.; Schmidt, T.; Bonnet, S. Water-Dispersible Silica-Coated Upconverting Liposomes: Can a Thin Silica Layer Protect TTA-UC against Oxygen Quenching? *ACS Biomater. Sci. Eng.* **2017**, *3* (3), 322–334. <https://doi.org/10.1021/acsbio materials.6b00678>.
- (47) Schloemer, T. H.; Sanders, S. N.; Zhou, Q.; Narayanan, P.; Hu, M.; Gangishetty, M. K.; Anderson, D.; Seitz, M.; Gallegos, A. O.; Stokes, R. C.; Congreve, D. N. Triplet Fusion Upconversion Nanocapsule Synthesis. *JoVE J. Vis. Exp.* **2022**, No. 187, e64374. <https://doi.org/10.3791/64374>.
- (48) Nishimura, N.; Gray, V.; Allardice, J. R.; Zhang, Z.; Pershin, A.; Beljonne, D.; Rao, A. Photon Upconversion from Near-Infrared to Blue Light with TIPS-Anthracene as an Efficient Triplet–Triplet Annihilator. *ACS Mater. Lett.* **2019**, *1* (6), 660–664. <https://doi.org/10.1021/acsmaterialslett.9b00287>.
- (49) Ng, L. V.; McCormick, A. V. Acidic Sol–Gel Polymerization of TEOS: Effect of Solution Composition on Cyclization and Bimolecular Condensation Rates. *J. Phys. Chem.* **1996**, *100* (30), 12517–12531. <https://doi.org/10.1021/jp960089o>.

- (50) Rankin, S. E.; Kasehagen, L. J.; McCormick, A. V.; Macosko, C. W. Dynamic Monte Carlo Simulation of Gelation with Extensive Cyclization. *Macromolecules* **2000**, *33* (20), 7639–7648. <https://doi.org/10.1021/ma000132c>.
- (51) Kasehagen, L. J.; Rankin, S. E.; McCormick, A. V.; Macosko, C. W. Modeling of First Shell Substitution Effects and Preferred Cyclization in Sol–Gel Polymerization. *Macromolecules* **1997**, *30* (13), 3921–3929. <https://doi.org/10.1021/ma9619142>.
- (52) Kalyanasundaram, K. *Photochemistry in Microheterogeneous Systems*; Academic Press: Orlando, 1987.
- (53) Saenz, F.; Ronchi, A.; Mauri, M.; Vadrucci, R.; Meinardi, F.; Monguzzi, A.; Weder, C. Nanostructured Polymers Enable Stable and Efficient Low-Power Photon Upconversion. *Adv. Funct. Mater.* **2021**, *31* (1), 2004495. <https://doi.org/10.1002/adfm.202004495>.
- (54) Zhou, Q.; Wirtz, B.; Schloemer, T.; Burroughs, M.; Hu, M.; Narayanan, P.; Lyu, J.; Gallegos, A.; Layton, C.; Mai, D.; Congreve, D. Spatially Controlled UV Light Generation at Depth Using Upconversion Micelles. **2022**. <https://doi.org/10.26434/chemrxiv-2022-8ppfr>.